

Simulating spatiotemporal aeolian sediment supply at a mega nourishment

Hoonhout, Bas; de Vries, Sierd

DOI

[10.1016/j.coastaleng.2018.12.007](https://doi.org/10.1016/j.coastaleng.2018.12.007)

Publication date

2019

Document Version

Accepted author manuscript

Published in

Coastal Engineering

Citation (APA)

Hoonhout, B., & de Vries, S. (2019). Simulating spatiotemporal aeolian sediment supply at a mega nourishment. *Coastal Engineering*, 145, 21-35. <https://doi.org/10.1016/j.coastaleng.2018.12.007>

Important note

To cite this publication, please use the final published version (if applicable).
Please check the document version above.

Copyright

Other than for strictly personal use, it is not permitted to download, forward or distribute the text or part of it, without the consent of the author(s) and/or copyright holder(s), unless the work is under an open content license such as Creative Commons.

Takedown policy

Please contact us and provide details if you believe this document breaches copyrights.
We will remove access to the work immediately and investigate your claim.

Simulating Spatiotemporal Aeolian Sediment Supply at a Mega Nourishment

Bas Hoonhout^{a,*}, Sierd de Vries^b

^a*Deltares, Department of Hydraulic Engineering, Boussinesqweg 1, 2629HV Delft, The Netherlands.*

^b*Delft University of Technology, Faculty of Civil Engineering and Geosciences, Department of Hydraulic Engineering, Stevinweg 1, 2628CN Delft, The Netherlands.*

Abstract

Mega nourishments are a novel approach to stimulating coastal safety and resilience. Mega nourishments are intended to spread along the coast on a decadal time scale by natural sediment transport processes with a minimum of intrusion into the natural coastal system. The supratidal morphodynamic behaviour of mega nourishments is not well understood due to complexities introduced by limitations in sediment availability to aeolian sediment transport. Consequently, the effectiveness of mega nourishments to stimulate coastal safety and to influence coastal landscape and habitat development remains unknown.

In this paper we present a detailed 4-year hindcast of the morphological development of the Sand Motor mega nourishment in The Netherlands. We use the aeolian sediment transport and availability model AEOLIS that focuses specifically on the simulation of spatiotemporal variations in sediment availability. The model includes the recurrence relation between sediment availability and aeolian sediment transport through self-grading and beach armoring.

We show that the model is able to reproduce multi-annual aeolian sediment transport rates in the Sand Motor domain in the four years after its construction. The RMSE is $3 \cdot 10^4 \text{ m}^3$ (7% of the total sediment accumulation) and R^2 is 0.93 when comparing timeseries of total sediment accumulation in the dunes, dune lake and lagoon. The combination of spatial and temporal

*Corresponding author

Email address: bas.hoonhout@deltares.nl (Bas Hoonhout)

variations in aeolian sediment availability, due to the combined influence of soil moisture, sediment sorting and beach armoring, is essential for an accurate estimate of the total sedimentation volume. The simulated feedback between aeolian sediment availability and transport is required for accurately describing compartmentalization of the beach and locating the aeolian sediment source areas in the Sand Motor domain.

Keywords: aeolian sediment transport; aeolian sediment supply; beach armoring; mega nourishment; Sand Motor; numerical model; aeolis

1. Introduction

Mega nourishments are a novel approach to stimulate coastal safety and resilience (Stive et al., 2013). By concentrating coastal interventions in both time and space, mega nourishments are believed to strengthen the natural coastal system and provide a cost-effective solution to coastal hazards with a minimum of intrusion into the natural coastal system. Mega nourishments are intended to spread along the coast on a decadal time scale by natural sediment transport processes, while stimulating natural coastal landscape and habitat development. Mega nourishment are flexible enough to cope with uncertainties associated with climate change. The Sand Motor in The Netherlands is the first implementation of a mega nourishment worldwide.

Past research at the Sand Motor revealed particular morphodynamic behaviour associated with mega nourishments that is not well understood (de Schipper et al., 2016; Huisman et al., 2016; Radermacher et al., 2017). Hoonhout and de Vries (2017) showed that the supratidal morphodynamic behavior of the Sand Motor mega nourishment is highly compartmentalized. The compartmentalization results in dune growth rates that are lower than along the adjacent coasts with more regular beaches. Despite beach widths up to 1 kilometer, aeolian sediment transport rates remain modest due to limitations in sediment availability.

Limitations in sediment availability complicate estimations of sediment fluxes based on aeolian sediment transport models (e.g. Jackson and Cooper, 1999; Lynch et al., 2008; Davidson-Arnott and Bauer, 2009; Aagaard, 2014). Consequently, aeolian sediment transport models systematically overestimate the actual aeolian sediment flux (Sherman et al., 1998; Sherman and Li, 2012). Limitations in sediment availability are traditionally incorporated in formulations for equilibrium or saturated sediment transport through a shear

velocity threshold (e.g. Howard, 1977; Dyer, 1986; Belly, 1964; Johnson, 1965; Hotta et al., 1984; Nickling and Ecclestone, 1981; Arens, 1996; King et al., 2005). But sediment availability is governed by a variety of environmental factors and inherently varies both in time and space. To incorporate the spatiotemporal variations in sediment availability, various conceptual frameworks have been developed.

Bauer and Davidson-Arnott (2002) introduced the concept of critical fetch to account for limitations in fetch and sediment availability and supply in coastal sediment transport estimates. de Vries et al. (2014a) used an explicit source term in a one-dimensional advection formulation to account for spatial variations in sediment availability. Keijsers et al. (2016) introduced the behavioral DUBEVEG model, as extension of the DECAL algorithm (Baas, 2002), that uses probabilities to account for spatiotemporal differences in beach erosion, dune development and vegetation growth. Although conceptually useful, these concepts have limited predictive capabilities as the critical fetch in Bauer and Davidson-Arnott (2002), the explicit source term in de Vries et al. (2014a) and the probabilities in the DUBEVEG model are typically unknown a-priori. Therefore, various process-based frameworks have been developed to simulate the spatiotemporal variation in sediment availability. The simulated sediment availability can then be fed to an aeolian sediment transport model to obtain aeolian sediment transport fluxes for availability-limited coastal systems.

Van Dijk et al. (1999) and Van Boxel et al. (1999) introduced an extensive numerical model that simulates airflow over a given topography and computes the spatiotemporal variation in aeolian sediment transport including various limitations in sediment availability, like the effect of precipitation and vegetation. Their model did not allow for simulation of the limitations in sediment availability itself and is computationally intensive due to the flow solver. Kroy et al. (2002) introduced a more lightweight flow solver based on the model of Weng et al. (1991). Durán and Moore (2013) extended this model with a vegetation growth model and a water line to simulate the development of coastal dunes. However, their model is focused on more traditional coastlines as simulation of sediment availability is included only through vegetation. Hoonhout and de Vries (2016) introduced the AEOLIS model that focuses specifically on the simulation of spatiotemporal variations in sediment availability, including the recurrence relation between sediment availability and aeolian sediment transport through self-grading and beach armoring. The model can be used to obtain a lightweight, but versatile aeo-

lian sediment transport model that is suitable for availability-limited coastal environments.

Practical and versatile aeolian sediment transport models with predictive skill are a prerequisite for design of mega nourishments. Optimization of designs on the effectiveness to increase coastal safety and resilience, while stimulating natural coastal landscape and habitat development, requires spatiotemporal differentiation of aeolian sediment transport and availability. To provide insight in the predictive skill of models for the long-term development of the complex coastal environments that mega nourishment typically are, long-term validation is required.

In this paper we present a detailed 4-year hindcast of the morphological development of the Sand Motor mega nourishment in The Netherlands using the aeolian sediment transport and availability model AEOLIS (Hoonhout and de Vries, 2016). We show that spatiotemporal variations in sediment availability cause compartmentalization of the mega nourishment and increase its lifetime significantly. We also show that both spatial and temporal variability in sediment availability are key to explain the long-term and seasonal morphodynamic behaviour of the nourishment.

2. Field Site

The Sand Motor (or Sand Engine) is an artificial 21 Mm³ sandy peninsula protruding into the North Sea off the Delfland coast in The Netherlands (Figure 1, Stive et al., 2013). The Sand Motor was constructed in 2011 and its bulged shoreline initially extended about 1 km seaward and stretched over approximately 2 km along the original coastline. The original coast was characterized by an alongshore uniform profile with a vegetated dune with an average height of 13 m and a linear beach with a 1:40 slope. The dune foot is located at a height of approximately 5 m+MSL.

Due to natural sediment dynamics the Sand Motor distributes about 1 Mm³ of sand per year to the adjacent coasts (Figure 1). The majority of this sand volume is transported by tides and waves. However, the Sand Motor is constructed up to 5 m+MSL and locally up to 7 m+MSL, which is in either case well above the maximum surge level of 3 m+MSL (Figure 2c). Therefore, the majority of the Sand Motor area is uniquely shaped by wind.

The Sand Motor comprises both a dune lake and a lagoon that act as large traps for aeolian sediment (Figure 1). The lagoon is affected by tidal forcing, although the tidal amplitude quickly diminished over time as the

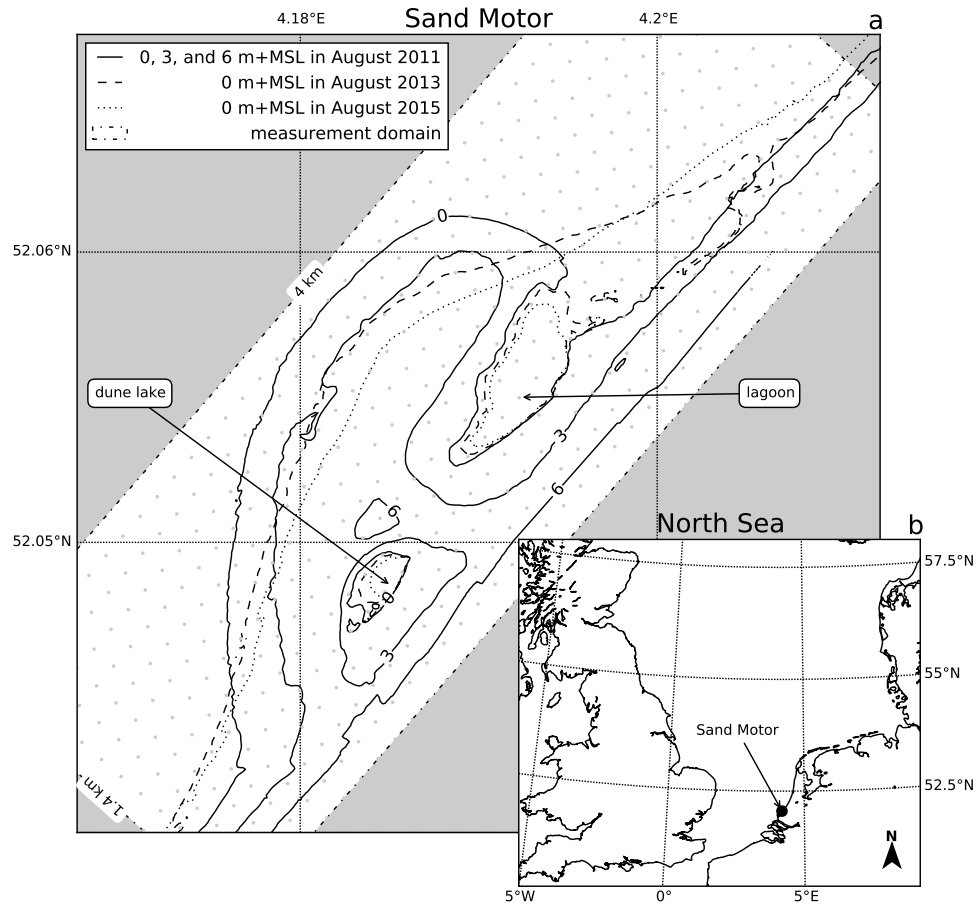


Figure 1: Location, orientation, appearance and evolution of the Sand Motor between construction in 2011 and 2015. The box indicates the measurement domain used in the remainder of this paper. A 100 x 100 m grid aligned with the measurement domain is plotted in gray as reference.

entry channel elongated. The tidal range of about 2 m that is present at the Sand Motor periphery (Figure 2c), is nowadays damped to less than 20 cm inside the lagoon (de Vries et al., 2015). Consequently, the tidal currents at the closed end of the lagoon, where most aeolian sediment is trapped, are negligible.

The dominant wind direction at the Sand Motor is south to southwest (Figure 2a). However, during storm conditions the wind direction tends to be southwest to northwest. During extreme storm conditions the wind direction tends to be northwest. Northwesterly storms are typically accompanied by significant surges as the fetch is virtually unbounded to the northwest, while surges from the southwest are limited due to the presence of the narrowing of the North Sea at the Strait of Dover (Figure 1, inset).

3. Model description

A two-dimensional (2DH) advection model for spatiotemporal varying aeolian sediment transport and availability is used (Hoonhout and de Vries, 2016). The model simulates sediment availability through the processes of sediment sorting, beach armoring and flooding and drying. For this purpose the bed is discretized in horizontal grid cells and in vertical bed layers (2DV) that move with the bed. Moreover, the grain size distribution is discretized into fractions. This allows the grain size distribution, sediment availability and sediment supply to vary both horizontally and vertically.

The model describes the instantaneous sediment mass per unit area in transport c [kg/m²] by an advection equation, which reads in one-dimensional notation:

$$\frac{\partial c_k}{\partial t} + u_z \frac{\partial c_k}{\partial x} = E_k - D_k \quad (1)$$

where t [s] denotes time, x [m] denotes the cross-shore distance from a zero-transport boundary, and k [-] denotes the sediment fraction index. u_z [m/s] is the wind velocity at height z [m]. E_k and D_k [kg/m²/s] represent the erosion and deposition terms and hence combined represent the net entrainment of sediment.

The net entrainment is determined based on a balance between the equilibrium or saturated sediment concentration $c_{\text{sat},k}$ [kg/m²] and the instantaneous sediment transport concentration c_k and is maximized by the available sediment in the bed $m_{a,k}$ [kg/m²] according to:

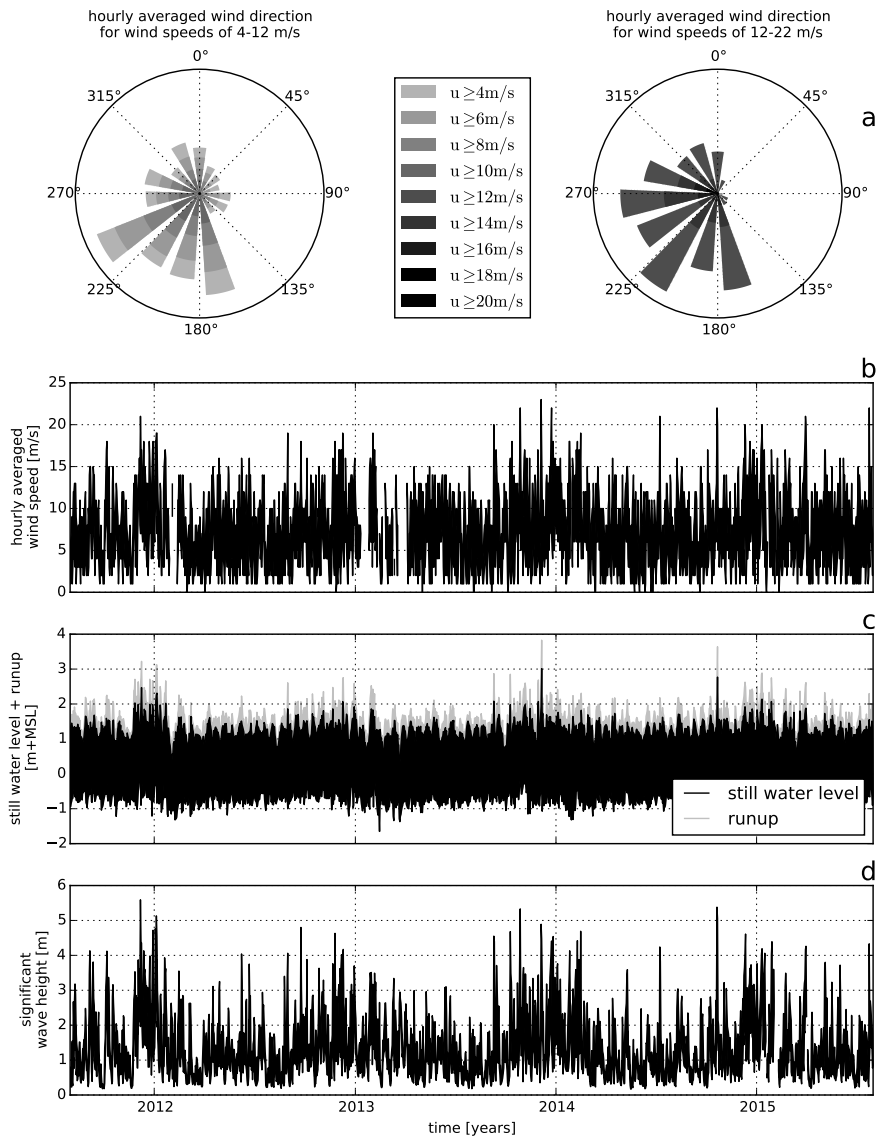


Figure 2: Wind and hydrodynamic time series from 2011 to 2015. Hourly averaged wind speeds and directions are obtained from the KNMI meteorological station in Hoek van Holland (upper panels). Offshore still water levels, wave heights and wave periods are obtained from the Europlatform (lower panels). Runup levels are estimated following Stockdon et al. (2006).

$$E_k - D_k = \min \left(\frac{\partial m_{a,k}}{\partial t} \quad ; \quad \frac{\hat{w}_k \cdot c_{\text{sat},k} - c_k}{T} \right) \quad (2)$$

where T [s] represents an adaptation time scale that is assumed to be equal for both erosion and deposition. \hat{w}_k is a weighting factor that sums to unity over the grain size fractions. The saturated sediment concentration $c_{\text{sat},k}$ is computed using an empirical sediment transport formulation (e.g. Bagnold, 1937).

The empirical sediment transport fomulation is provided with a term for the shear velocity threshold $u_{*th,k}$ [m/s] that defines the minimum wind shear required to initiate and sustain saltation transport. The shear velocity threshold is determined based on bed surface properties, like soil moisture content and the presence of roughness elements.

Saturation of the soil is assumed to be instantaneous with rising tide. The drying of the beach surface through infiltration is assumed to follow an exponential decay. In order to capture this behavior the volumetric water content is implemented according to:

$$p_V = \begin{cases} p & \text{if } \eta > z_b \\ p \cdot \int e^{\frac{\log(0.5)}{T_{\text{dry}}} \cdot dt} & \text{if } \eta \leq z_b \end{cases} \quad (3)$$

where p [-] is the porosity, η [m+MSL] is the instantaneous water level, z_b [m+MSL] is the local bed elevation, p_V [-] is the volumetric water content. T_{dry} [s] is the beach drying time scale, defined as the time in which the beach moisture content halves.

Waves cause stirring of the bed and mixing of the sediment that is available in the vertical bed layers. Therefore, wave action can cause finer sediment in deeper bed layers to surface thereby increasing local sediment availability. However, also in case of wave action sediment availability is limited as the model does not include a marine sediment source.

The sheltering effect of roughness elements protruding from the bed and affecting the local wind shear and shielding local sediment is implemented following Raupach et al. (1993):

$$f_{u_{*th,R}} = \sqrt{(1 - m\sigma\lambda)(1 + m\beta\lambda)} \quad (4)$$

where $f_{u_{*th,R}}$ [-] is a factor with which the local instantaneous shear velocity threshold per sediment fraction is multiplied. λ [-] is the roughness density.

m , β and σ [-] are empirical factors defined in Raupach et al. (1993) representing the difference between mean and maximum shear stress, the ratio between the drag coefficient of the roughness elements alone and the drag coefficient of the unarmored sandy bed, and the ratio between the basal and frontal area of the roughness elements respectively.

Due to the implementation of multi-fraction sediment transport (Equations 1 and 2), fine sediment is eroded from the bed surface more easily than coarse sediment. Consequently, the bed surface coarsens over time. The implementation of the sheltering effect of roughness elements (Equation 4) enhances this effect as also roughness elements surface over time and limit sediment availability in erosive zones. Currently, the only counteracting process implemented in the model is wave stirring. Other processes, like weathering, abrasion, breakage or mobilization of larger shell fragments are not included, but tend to act on a larger temporal scale or occur irregularly.

4. Model approach

The two-dimensional (2DH) model of the Sand Motor is constructed and calibrated based on four years of field measurements on wind, tides, waves and topography. The calibrated model is used to investigate the influence of spatiotemporal variations in aeolian sediment availability on sediment accumulation in the Sand Motor domain.

To test that the Sand Motor mega nourishment is indeed an availability-limited coastal system, the measured long-term sediment accumulation volumes (Hoonhout and de Vries, 2017) are first compared to a reference model that assumes no limitations in sediment availability exist.

4.1. Reference model

A selection of equilibrium sediment transport formulations is used as reference model. An equilibrium sediment transport formulation describes the wind transport capacity in given conditions. In conjunction with a shear velocity threshold based on only a constant uniform median grain size, an estimate of the potential aeolian sediment accumulation in absence of availability-limitations can be obtained. The potential aeolian sediment accumulation or cumulative wind transport capacity Q [m³] in the Sand Motor domain is estimated based on hourly averaged time series of the wind speed u_z [m/s] and direction θ_u [°] obtained from the KNMI meteorological station in Hoek van Holland following:

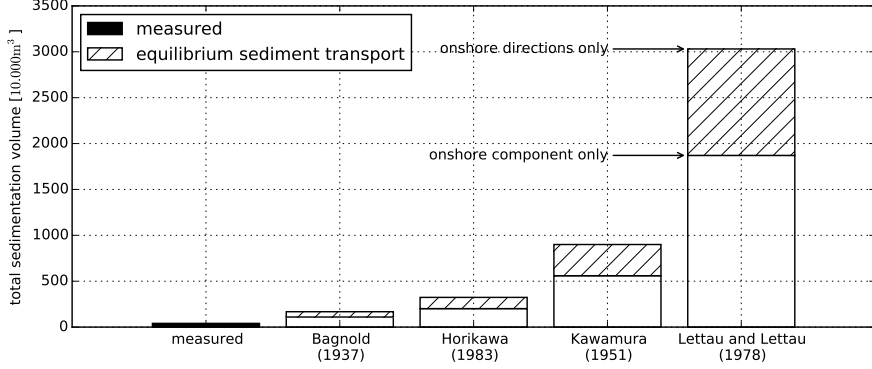


Figure 3: Comparison of the cumulative wind transport capacity according to a selection of equilibrium sediment transport formulations and measured total sedimentation in the Sand Motor domain. The equilibrium sediment transport is based on an hourly averaged wind speed and direction time series from September 1, 2011 until September 1, 2015. Offshore wind directions are discarded. For the upper boundary of each estimate all wind directions are weighted equally. For the lower boundary of each estimate the wind directions are weighted according to the magnitude of the onshore component.

$$Q = \sum q \cdot \frac{\Delta t \cdot \Delta y}{(1-p) \cdot \rho_p} \cdot f_{\theta_u} \quad (5)$$

where the temporal resolution $\Delta t = 1$ h, the alongshore span of the domain $\Delta y = 4$ km, the porosity $p = 0.4$, the particle density $\rho_p = 2650$ kg/m³, the sediment transport rate q is given by the equilibrium sediment transport formulation (Table 1) and f_{θ_u} is a factor to account for the wind direction. The wind direction can be accounted for by only including the onshore wind component with respect to the original coastline orientation. However, given the typical Sand Motor geometry (Figure 1), sediment is likely to be trapped in the dune lake and lagoon even with alongshore wind. Therefore it can be assumed that the onshore wind component will provide a lower limit of the cumulative wind transport capacity. Similarly, an upper limit can be obtained by assuming that all onshore wind directions contribute equally to the cumulative wind transport capacity. For the upper limit the factor f_{θ_u} is defined as:

$$f_{\theta_u} = \begin{cases} 1 & \text{if } \cos(312^\circ - \theta_u) \geq 0 \\ 0 & \text{if } \cos(312^\circ - \theta_u) < 0 \end{cases} \quad (6)$$

while for the lower limit the factor f_{θ_u} is defined as:

$$f_{\theta_u} = \max(0 ; \cos(312^\circ - \theta_u)) \quad (7)$$

where 312° accounts for orientation of the original coastline. Figure 3 presents an overview of the cumulative wind transport capacity in the Sand Motor domain over the period between September 1, 2011 and September 1, 2015 according to a selection of equilibrium sediment transport formulations and in comparison with the measured accumulation volumes. The estimates of the wind transport capacity show a large variation between formulations that are mainly due to the incorporation of the shear velocity threshold. However, all formulations overestimate the measured sediment accumulation in the Sand Motor domain with at least a factor 3 – 4. The large variation and consistent overestimation is in accordance with the review of aeolian sediment transport models presented by Sherman and Li (2012). The consistent overestimation of the measured sedimentation volumes in the Sand Motor domain suggest that the Sand Motor is indeed an availability-limited coastal system.

4.2. Schematization

A two-dimensional (2DH) aeolian sediment availability and transport model for the Sand Motor mega nourishment is constructed for the four years between September 1, 2011 and September 1, 2015, which is shortly after the nourishment was placed. The model’s topography and grid are based on the measured topographies of August 3, 2011 and later. The topographies are rotated 48° and interpolated to a 50 x 50 m grid spanning 1.5 km cross-shore and 4 km alongshore with respect to the original coastline, not including the dunes (Figure 4, upper panel).

Four years of hourly wind speed and direction data measured at 10 m above the bed is obtained from the KNMI meteorological station at Hoek van Holland (Figure 2a,b) are uniformly imposed to the model.

An average lognormal grain size distribution with a median diameter $d_{50} = 335 \mu\text{m}$ is used as measured at the Sand Motor field site. The sand fractions cover a range from 0.1 to 2 mm. The amount of shells and other roughness elements in the originally nourished sand is estimated to be 5%. The estimate is based on three sediment samples obtained from the field site 0.5 m below the bed surface. Additional fractions ranging from 2 to 32 mm are added according to a lognormal distribution to account for the

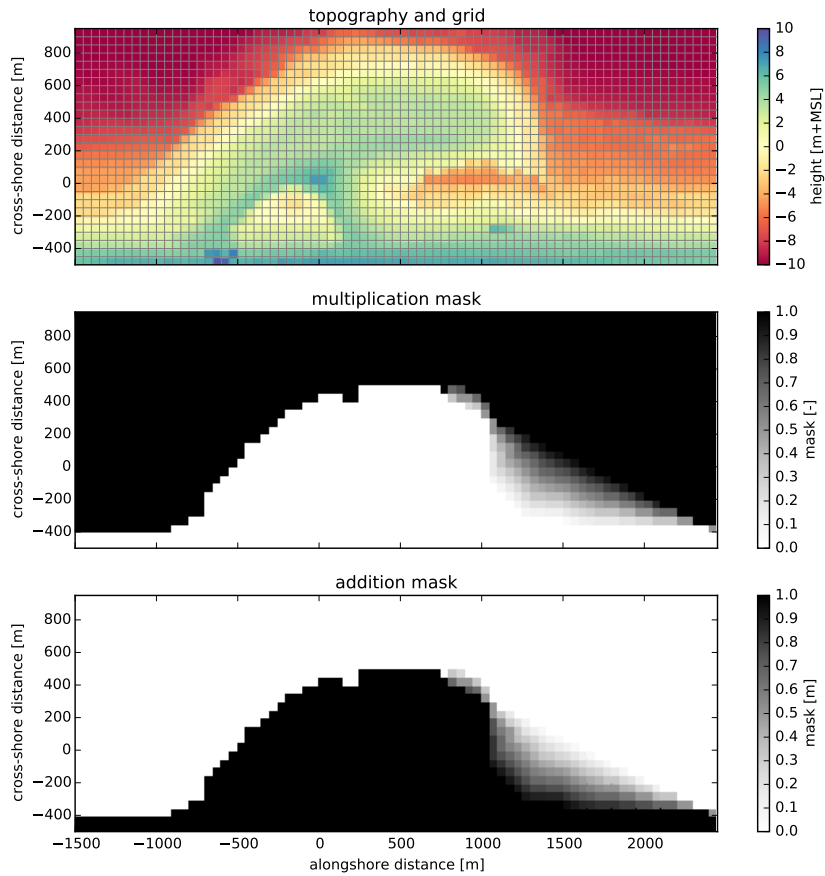


Figure 4: Model grid and topography based on the topographic survey of August 3, 2011 (upper panel) and hydrodynamic mask used to limit tidal and wave motions in the dune lake and lagoon (middle and lower panels). Water levels and wave heights are uniformly imposed to the model and multiplied by the multiplication mask and subsequently increased with the addition mask.

Table 1: Equilibrium sediment transport formulations, coefficient values* and the ratio between measurements and model results.

Reference	Equation	C	Ratio
Bagnold (1937)	$q = C \frac{\rho_a}{g} \sqrt{\frac{d_n}{D_n}} (u_* - u_{*th})^3$	1.8	3 – 4
Horikawa et al. (1983)	$q = C \frac{\rho_a}{g} (u_* + u_{*th})^2 (u_* - u_{*th})$	1.0	5 – 8
Kawamura (1951)	$q = C \frac{\rho_a}{g} (u_* + u_{*th})^2 (u_* - u_{*th})$	2.78	14 – 22
Lettau and Lettau (1978)	$q = C \frac{\rho_a}{g} \sqrt{\frac{d_n}{D_n}} (u_* - u_{*th}) u_*^2$	6.7	46 – 75

* Other values are the shear velocity $u_* = \alpha \cdot u_z$ m/s, the shear velocity threshold $u_{*th} = \alpha \cdot 3.87$ m/s, the conversion factor from free-flow wind velocity to shear velocity $\alpha = 0.058$, the air density $\rho_a = 1.25$ kg/m³, the particle density $\rho_p = 2650.0$ kg/m³, the gravitational constant $g = 9.81$ m/s², the nominal grain size $d_n = 335$ μ m, a reference grain size $D_n = 250$ μ m and the height above the bed of the wind measurement $z = 10$ m.

presence of roughness elements in the bed. The grain size distribution is used to populate the initial bed that consists of 10 bed composition layers with a thickness of 1 cm each.

The hindcast aims at the large scale and long term sedimentation volumes as presented by Hoonhout and de Vries (2017). Therefore an efficient, but diffusive, implicit Euler Backward scheme with a timestep of 1 h is used that does not resolve high frequency variations in wind or sediment transport. Consequently, the model produces smooth solutions that describe hourly steady states based on the instantaneous average wind speed and sediment availability.

Bagnold (1937) is selected as equilibrium sediment transport formulation as it is derived separately for different grain sizes and therefore suitable for multi-fraction aeolian sediment transport. Alternative formulations (Table 1) are derived for wider grain size distributions that do not necessarily result in a monotonic relation between the grain size and the sediment transport rate (e.g. Kawamura, 1951; Horikawa et al., 1983). Such non-monotonic relation is unrealistic in a multi-fraction context as it would result in a preference to transport both fine sediment and large elements that are considered non-erodible. Moreover, the formulation of Bagnold (1937) overestimates the measured aeolian sediment transport rates in the Sand Motor domain less compared to alternative formulations (Table 1, rightmost column).

Hourly offshore water levels and wave heights are obtained from the Eu-

roplatform for the same period (Figure 2c,d). and are initially uniformly imposed to the model. Consequently, the tidal range, mean water level and wave heights that are present at the Sand Motor periphery are also present in the dune lake and lagoon. In reality, the tidal range and wave heights in the dune lake and lagoon are much lower, while the mean water level in the dune lake and lagoon is elevated compared to mean sea level (de Vries et al., 2015). To account for these spatial differences in hydrodynamics a hydrodynamic mask is applied (Figure 4, middle and lower panel).

Subtidal changes in topography are not simulated by the model. The subtidal changes can be important to aeolian sediment transport as the location and size of aeolian sediment erosion and deposition areas might change. To account for these changes, measured topographies are imposed to the model through a Basic Model Interface (BMI, Peckham et al., 2013).

All measured topographies in the period between September 1, 2011 and September 1, 2015 are linearly interpolated in time as to obtain daily updates of the Sand Motor’s topography. The hydrodynamic mask is updated along with the topography. The presented aeolian sediment transport rates are based on the time-integrated entrainment and deposition rates that are computed by the model rather than differences in topography.

4.3. Calibration

The model is calibrated on the shape of roughness elements that emerge from the bed and shelter the sand surface from wind erosion, the drying rate of the soil and the time needed for the sediment transport to adapt to changing wind conditions. These processes are represented in the model by parameters for which data or literature can only provide approximate values:

1. σ , as used in the formulation of Raupach et al. (1993, Equation 4), is the ratio between the basal and frontal area of the roughness elements that constitute the beach armor layer.
2. T_{dry} is the time scale at which the beach dries out after flooding (Equation 3). It represents the time in which the soil moisture content halves in case the beach is not inundated and no evaporation occurs.
3. T is the adaptation time scale in the right-hand side of the advection equation (Equation 2). It represents the time scale to which the sediment transport adapts to variations in the wind conditions and sediment availability.

The implementation of roughness elements is characterized by three calibration parameters: m , β and σ (Equation 4). m is a factor to account for the difference between the mean and maximum shear stress and is usually chosen as 0.5 for field applications (Raupach et al., 1993; McKenna Neuman et al., 2012). Numerically it is irrelevant if β or σ is calibrated as they only appear as a ratio $\frac{\beta}{\sigma}$ in the model implementation. As β is the ratio between the drag coefficient of the roughness elements alone and the drag coefficient of the unarmored sandy bed, the value can be assumed to be reasonably generic. In contrast, σ depends on the shape and protrusion of the roughness elements and therefore depends on the field site and varies in time. For example, a spherical object placed on top of the bed would be represented by $\sigma = 1$, while a spherical object protruding halfway through the bed (hemisphere) would be represented by $\sigma = 2$. Consequently, calibration of σ seems to be preferable as it is less certain. Wind tunnel experiments presented by McKenna Neuman et al. (2012) investigated the influence of lag deposits, consisting of shells and shell fragments, on aeolian sediment transport. Values for the calibration coefficients m and β were found to be 0.5 and 130 respectively and are adopted for the Sand Motor hindcast. An optimal average value for σ is obtained by systematic variation between 2 and 20.

The drying rate of the beach (T_{dry}) depends on many factors, like grain size, soil moisture content, groundwater level, wind speed and solar radiation. The use of a single time scale as aggregate for these processes is an oversimplification of reality. Therefore a wide range of parameter values is covered in the calibration. T_{dry} is varied between 0.1 and 10 hours where the former results in virtually instant drying and the latter results in an intertidal beach that is permanently too moist for aeolian sediment transport to be initiated.

The adaptation time scale (T), that represents the swiftness of aeolian sediment transport to adapt to changing wind conditions, is in the order of seconds (Davidson-Arnott et al., 2008; de Vries et al., 2014b). As the model time step is orders of magnitude larger, the model effectively solves steady states and the value for T will not affect temporal variations in sediment transport. However, the adaptation time scale also affects the development of the saltation cascade in space. Sediment transport increases in downwind direction from a zero-flux boundary, like the water line in case of onshore wind, with a rate that is governed by the value of T . Consequently, T influences the width of the source area in case of abundant sediment availability.

T is varied between 1 and 10 seconds.

The calibration is performed based on the bi-monthly erosion and deposition volumes as measured in the Sand Motor domain (Hoonhout and de Vries, 2017). The erosion and deposition volumes are determined within seven predefined zones (Figure 5) that aim to separate areas with marine influences (marine zone, mixed zone and lagoon) from areas without marine influences (aeolian zone, dune lake and dunes), and separate areas with net aeolian erosion (mixed and aeolian zone) from areas with net aeolian deposition (lagoon, dune lake and dunes). The zonation is based on the 0, 3 and 5 m+MSL contour lines that roughly correspond with the mean water level, maximum runup level or berm edge and the dune foot respectively. Note that zonation is strictly used as method to detail the spatial varying performance of the model. All modeled processes are identical throughout the computational domain. Zonation is not imposed to the model other than, indirectly, through topology. The average R^2 value of the time series for erosion and deposition is used as benchmark. The R^2 value represents the fraction of explained variance and is defined as:

$$R^2 = 1 - \frac{\sum_n [V_{\text{measured}}^n - V_{\text{model}}^n]^2}{\sum_n [V_{\text{measured}}^n - \overline{V_{\text{measured}}^n}]^2} \quad (8)$$

where V^n is the measured or modeled sediment volume in time period n . The overbar denotes time-averaging. In addition the root-mean-square error (RMSE) is presented as absolute measure for the model accuracy, which is defined as:

$$RMSE = \sqrt{\sum_n [V_{\text{measured}}^n - V_{\text{model}}^n]^2} \quad (9)$$

The calibration itself is performed in three steps:

1. A coarse calibration on σ and T_{dry} .
2. A calibration on T using the provisional optimal settings for σ and T_{dry} .
3. A fine calibration on σ and T_{dry} using the optimal setting for T .

5. Results

The optimal model settings were chosen from 150 realizations (Figure 6). The optimal realization has an R^2 value of 0.93 and a RMSE of $3 \cdot 10^4 \text{ m}^3$. The

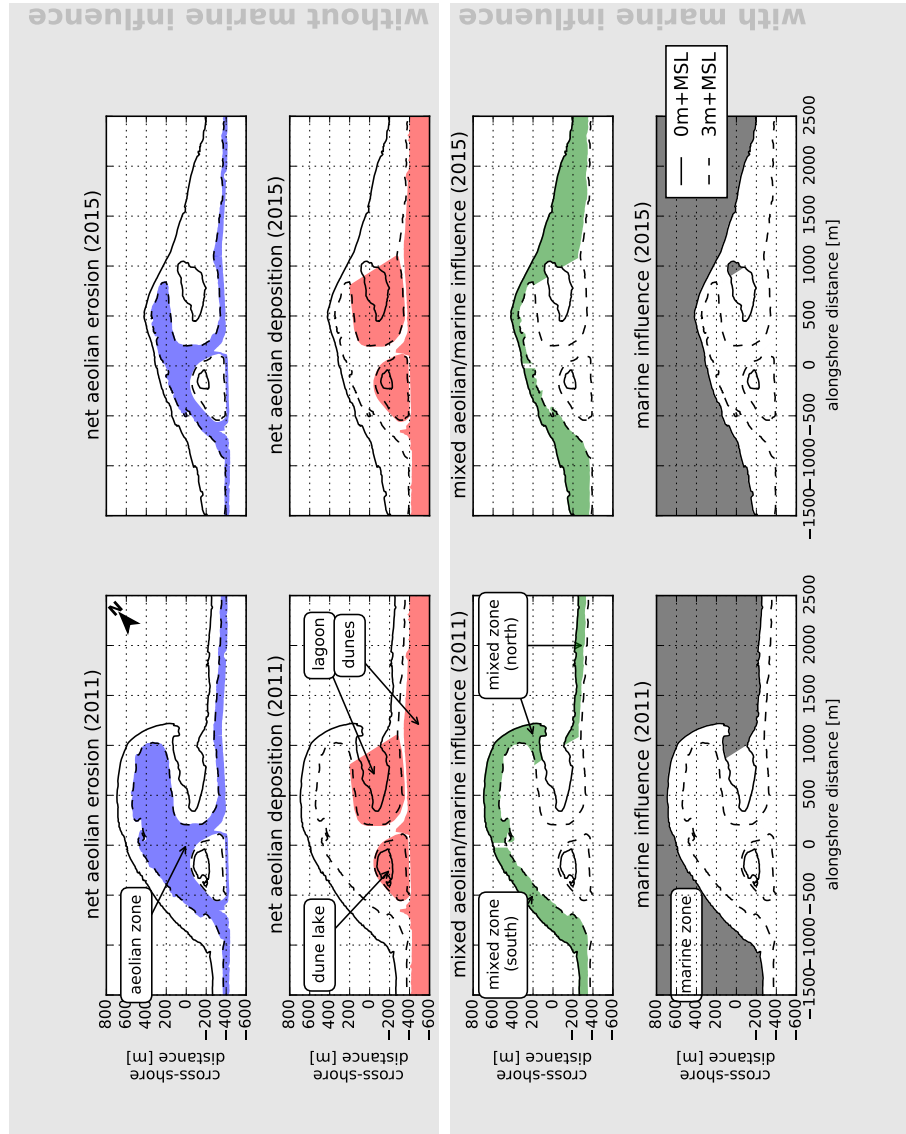


Figure 5: Zonation of the Sand Motor domain into zones with net aeolian erosion and no marine influence, net aeolian deposition and no marine influence, mixed aeolian/marine influence and marine influence. Zonation is based on the 0, 3 and 5 m+MSL contour lines that roughly correspond with the mean water level, maximum runup level or berm edge and the dune foot respectively. Left panels: 2011. Right panels: 2015. Source: Hoonhout and de Vries (2017).

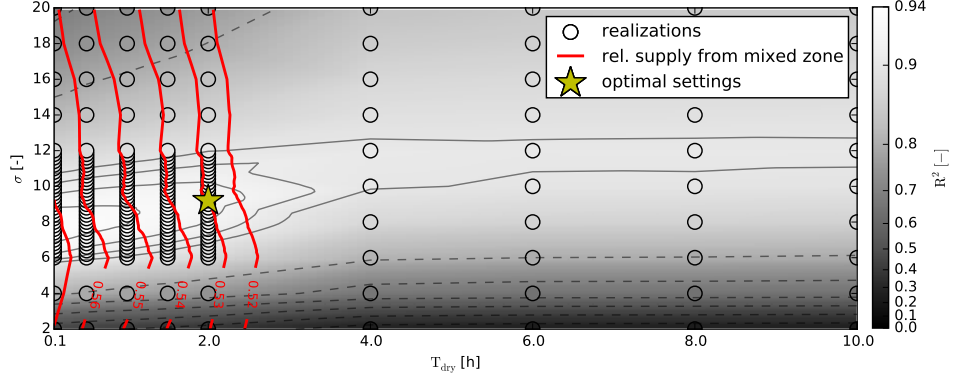


Figure 6: Systematic variation of calibration parameters σ and T_{dry} with $T = 1$ s. The circles indicate the realizations made. The colored background depicts a linear interpolation of the R^2 values with respect to the measurement data presented in Hoonhout and de Vries (2017) and Figure 8. The solid isolines depict R^2 values from 0.90 to 0.93, while the dashed isolines depict R^2 values from 0.0 to 0.9. The red lines depict the relative supply from the mixed zones ranging from 52% to 57%. The yellow star indicates the optimal value model settings.

corresponding optimal parameter settings are found to be $\sigma = 9.2$, $T_{\text{dry}} = 2$ h and $T = 1$ s. These settings were ultimately selected from a cluster of realizations with comparable R^2 values based on the relative sediment supply from the mixed zones (Figure 5, third row) at the end of the simulation. An overview of all model settings for the calibrated model is given in Appendix A.

Figure 7 shows that erosion from the aeolian zone (Figure 5, first row) is most pronounced in the first year and least in the second year in both the measurements and the model results. Also the deposition of aeolian sediment in the dune lake and lagoon (Figure 5, second row) is observed in both the measurements and model results, although the model underestimates these deposited volumes. The deposition in the dune lake and lagoon is also more localized in the measurements than in the model results. The spatial variability in the erosion of the aeolian zone is larger in the measurements than in the model results. The large variability measured in the mixed zone is not present in the model results as hydrodynamic sediment transport is not simulated.

The development of the total erosion and deposition volumes in the Sand Motor domain in the four year period is represented well by the model (Figure

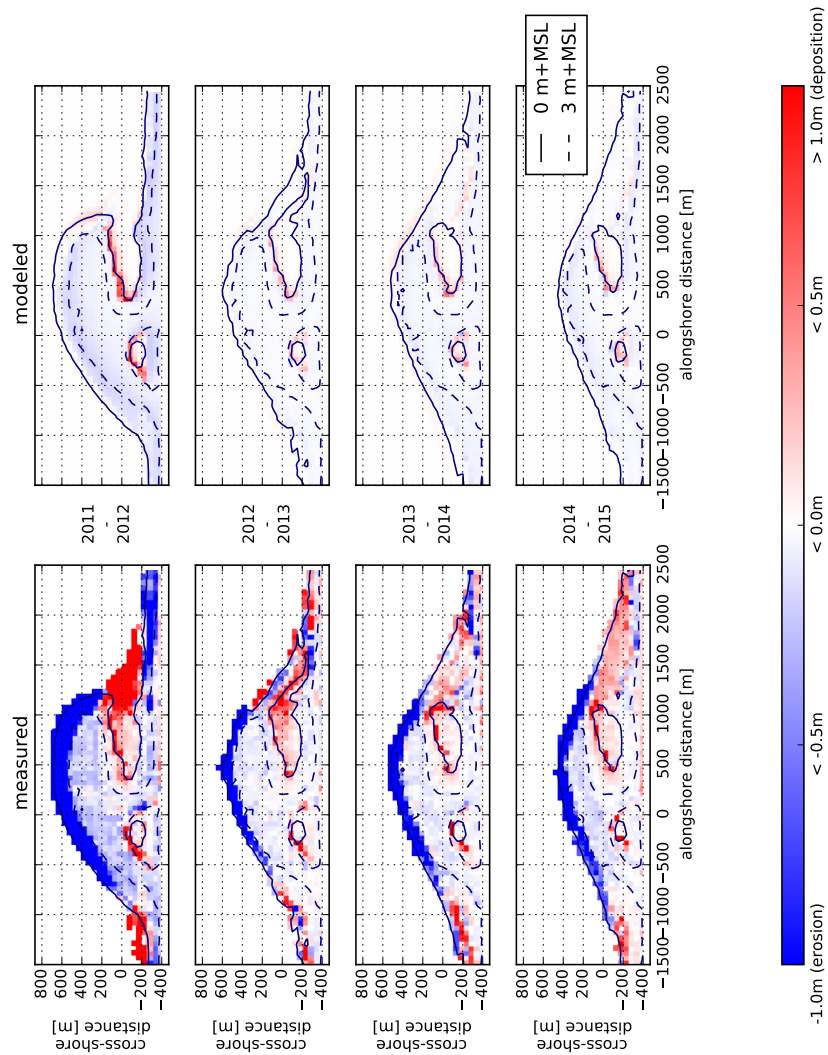


Figure 7: Simulated and measured yearly sedimentation and erosion above 0 m+MSL. Model results only include aeolian sediment transport as hydrodynamic sediment transport is not computed. Comparisons are made between the September surveys of each year.

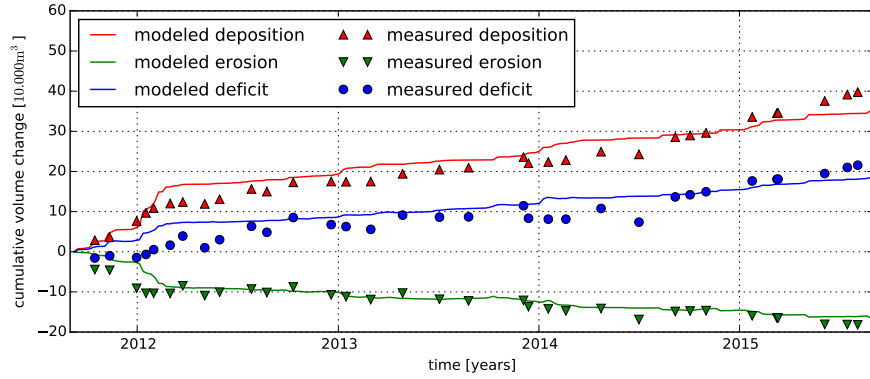


Figure 8: Simulated net volume change of erosion and deposition volumes compared to measured net volume change as presented in Hoonhout and de Vries (2017).

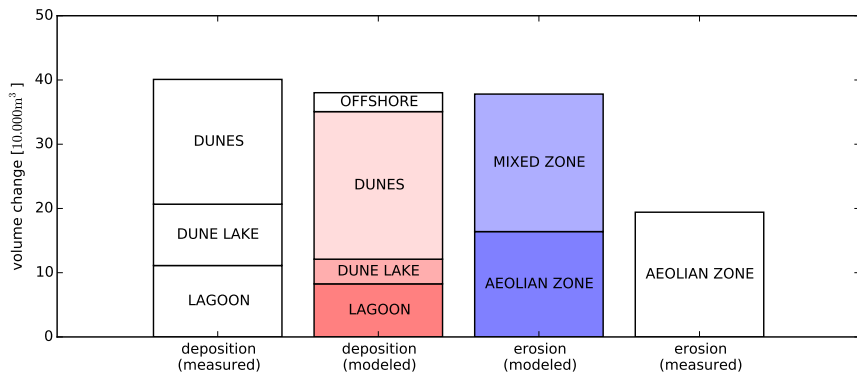


Figure 9: Total erosion and deposition volumes at the end of the simulation and measured total erosion and deposition volumes as presented in Hoonhout and de Vries (2017).

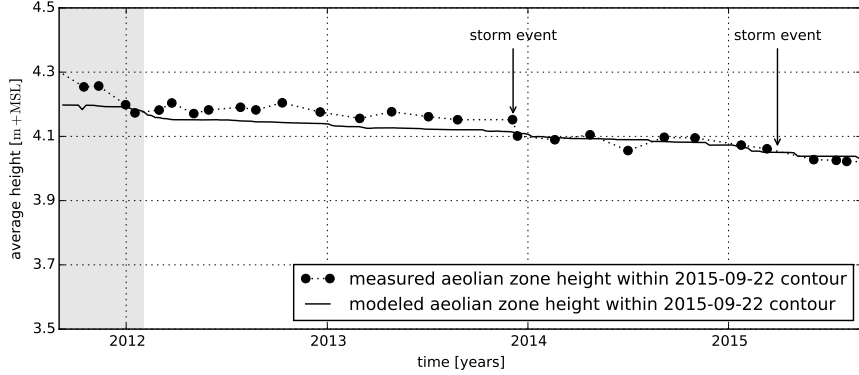


Figure 10: Simulated average beach height in the aeolian zone compared to measured average beach height as presented in Hoonhout and de Vries (2017).

8). The dune accumulation volume is overestimated at the expense of the sediment volumes deposited in the dune lake and lagoon (Figure 9). As the dune area is not included in the model domain, the sediment flux over the onshore boundary is assumed to settle in the dunes entirely. The total sediment accumulation at the end of the simulation is underestimated by 12% as the offshore sediment deposits are not included in the large scale sediment budget analysis that are used for comparison. The underestimation is unique for the last nine months of the simulation as the model overestimates the total sediment accumulation with 5% on average (Figure 8). The relative importance of the mixed zone as supplier of aeolian sediment is well captured.

The change in beach height within the most recent 3 m+MSL contour, that marks the aeolian zone, is represented by the model as the R^2 value is 0.71 and the RMSE is about 4 cm or 12% of the average bed level change (Figure 10). As the change in beach height is computed within the most recent 3 m+MSL contour, the discrepancy is illustrative for the differences in spatial variability in erosion between measurements and model results. The lowering of the beach in the aeolian zone in the first half year of the simulation is particularly underestimated, while the accelerated erosion in this period is well captured in the total sediment transport. This indicates that sediment is eroded from outside the most recent 3 m+MSL contour.

The coverage of non-erodible elements $\lambda\sigma$ [-] (Equation 4) in the aeolian zone varies between 60% and 80% at the end of the simulation. The coverage is high compared to the 10% – 20% shell coverage estimated to be present

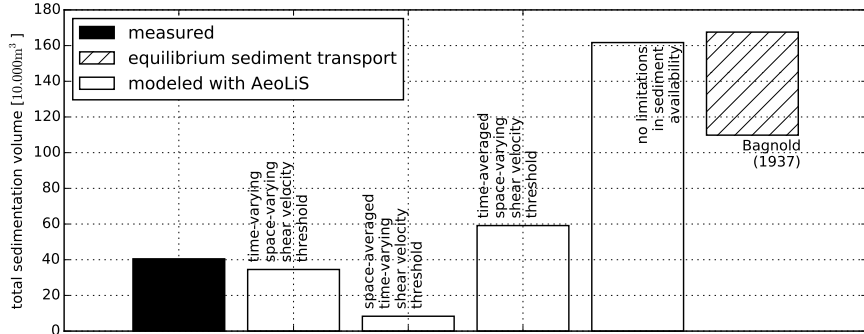


Figure 11: The influence of time-varying and space-varying shear velocity thresholds on the total sedimentation volume. The two leftmost bars depict the measured and modeled sedimentation volume as obtained from the calibrated model (Figure 9). The middle two bars depict results from two separate model simulations in which a space-averaged threshold time series or a time-averaged threshold field is imposed respectively. The former neglects compartmentalization, the latter neglects periodic flooding. The threshold averages are based on the result from the calibrated model. The two rightmost columns depict a result from a separate model simulation with a constant uniform threshold based on only a constant uniform median grain size and the estimated equilibrium sediment transport following Bagnold (1937) respectively (Table 1).

at the Sand Motor above 3 m+MSL based on gridded photographs.

Both the spatial and temporal variations in aeolian sediment availability are crucial for an accurate description of the compartmentalization of the Sand Motor. Compartmentalization governs both the total sedimentation and erosion volumes and the location of the aeolian sediment source and deposition areas. Figure 11 compares the total sedimentation volume according to measurements, the calibrated model and additional simulations, that are variations of the calibrated model in which spatial and/or temporal variations in the shear velocity threshold are averaged out. During these additional simulations the shear velocity threshold is not computed by the model, but space- and/or time-averaged thresholds based on the model results of the calibrated model are imposed. Negligence of the spatial variations results in an absence of compartmentalization and a 79% underestimation of the total sedimentation volume and a relative contribution of 8% of the mixed zones. The negligence of the temporal variations results in conservation of the compartmentalization, but an increased contribution of 86% of the mixed zones.

The total sedimentation volume is 46% overestimated in this case. In addition, a simulation without limitations in sediment availability overestimates the measured total sedimentation volumes with 400%, which is comparable to the wind transport capacity following Bagnold (1937, Figure 3).

6. Discussion

The model results show that multi-annual aeolian sediment erosion and deposition volumes, and the relative importance of the mixed zones as source of aeolian sediment are reproduced with reasonable accuracy. This suggests that indeed significant limitations in sediment availability, due to soil moisture content and beach armoring, govern aeolian sediment transport in the Sand Motor domain. A comparison with a simulation without limitation in sediment availability suggests that aeolian sediment availability in the Sand Motor domain is limited to about 25% – 35% of the wind transport capacity.

The negligence of spatial variations causes the model to underestimate the measured total sedimentation volume. The sediment supply from the relatively small mixed zone is marginalized as the imposed space-averaged shear velocity threshold is relatively high. In contrast, the negligence of temporal variations causes the model to overestimate the measured total sedimentation volume. The sediment supply from the mixed zones is increased as the effect of its periodic flooding is averaged out. At the same time, the sediment supply from the aeolian zone is decreased as the influence of beach armoring affects sediment availability from the start of the simulation rather than after the development of the beach armor layer. Therefore, the total sedimentation volume is not only overestimated, but also the importance of the mixed zones as supplier of aeolian sediment. This suggests that compartmentalization indeed govern the location of the aeolian sediment source and deposition areas and the total sediment accumulation in the Sand Motor domain.

6.1. Seasonal and local variations in sedimentation and erosion

The model can reproduce multi-annual trends in sedimentation volume, which is the aim of the hindcast, but seasonal and local variations are sometimes not represented by the model. An analysis of these variations is interesting as they influence the accuracy of specific model results.

Average wind speeds tend to be elevated in December and January (Figure 2), which leads to short periods of accelerated sediment accumulation in the beginning of 2012, 2013 and 2015 that are captured well by the model.

Early 2014 no accelerated sediment accumulation is measured, while the model simulation shows an increase in sediment accumulation originating from the mixed zones similar to other years.

The discrepancy early 2014 might be explained by topographic changes induced by hydrodynamic forces. On December 5th, 2013 an exceptional storm hit the Dutch coast. During this storm a significant decrease in aeolian deposits in the lagoon was observed, while deposits in the dunes and dune lake increased only marginally. The assumption that the closed end of the lagoon is mainly governed by aeolian sediment transport might be violated in these exceptional conditions. At the same time, the erosion of the aeolian zone that day equaled the total erosion of the aeolian zone that year. Consequently, the total subaerial sediment volume decreased that day with about $1 \cdot 10^4 \text{ m}^3$, possibly caused by hydrodynamic forces. This suggests that the simplified hydrodynamics, despite the use of a hydrodynamic mask, are a limiting factor in describing the Sand Motor's subaerial morphodynamics during extreme storms.

In the first months of the simulation, the total sediment accumulation is well represented, but erosion of the aeolian zone is underestimated. As beach armoring is the most important availability limitation in the aeolian zone, this suggests that the armoring rate is overestimated by the model. The armoring rate is mainly influenced by initial shell fraction of 5%, which might be overestimated, or the initially uniform distribution of shells in the bed is not an accurate representation of reality. Alternatively, processes that are not included in the model, like weathering, abrasion, breakage or mobilization of larger shell fragments, might explain the difference between model results and measurements. As weathering, abrasion and breakage affect the beach armoring on a larger temporal scale, mobilization of shells and shell fragments seems to be a more likely explanation to the discrepancies in the first months of the simulation.

Measured erosion and deposition rates exceed modeled erosion and deposition rates in the final nine months of the simulation. In this period dune growth seems to accelerate, while neither the deposition in the dune lake and lagoon did accelerate nor did the wind speed increase. The apparent acceleration is therefore solely found in the half yearly lidar measurements of the dune area (Hoonhout and de Vries, 2017) and is consequently based on a single data point. Despite the uncertainty involved in the measured acceleration, also precipitation rates, that were up to 70% lower in this period compared to the same period in other years, might explain the discrepancy at

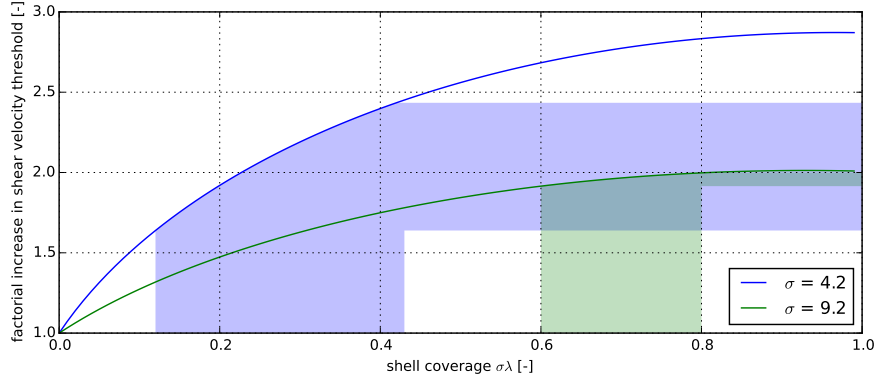


Figure 12: Relation between shear velocity threshold, shell coverage and σ according to Raupach et al. (1993, Equation 4). The shaded areas indicate the relevant parameter ranges from McKenna Neuman et al. (2012) (blue) and the model results (green).

the end of the simulation (Jackson and Nordstrom, 1998). For the hindcast no precipitation time series are imposed as the effect on the aeolian sediment transport rate is not properly understood yet. Consequently, the calibration of the model might have resulted in an overestimated importance of beach armoring to compensate for the negligence of precipitation.

The distribution of the aeolian sediment deposits over the dune lake, lagoon and dunes is not represented well as deposits in the dune lake and lagoon are underestimated. Additional hydrodynamic and hydrologic processes, like wind setup and groundwater seepage, might cause the entrapment area in reality to be larger than modeled. But more importantly, the dune lake and lagoon are positioned in the lee of the Sand Motor crest with respect to the predominant southwesterly wind direction. The height difference between the Sand Motor crest and the water level in the lagoon and dune lake is several meters, which is likely to influence the local wind field significantly. The probable decrease in wind shear in the lee of the Sand Motor crest promotes deposition of aeolian sediment and likely hampers supply to the dunes. These local variations in wind shear are not included in the simulations.

6.2. Beach armoring, sediment availability and the shear velocity threshold

The influence of beach armoring is reflected in the model by both σ and the roughness density λ (Equation 4). The optimal value for σ was found to be 9.2, which is high compared to the value of 4.2 found by McKenna Neuman

et al. (2012). The difference suggests that the roughness elements at the Sand Motor protrude less from the bed compared to what was found in the wind tunnel experiments. Consequently, the importance of beach armoring would be relatively low and compartmentalization of limited influence at the Sand Motor. However, the low σ value is largely compensated by the roughness density λ reflected in a shell coverage $\sigma\lambda$ that is high compared to what was found in the wind tunnel experiments (12% – 43% on average) and what is found at the Sand Motor field site (10% – 20%). Figure 12 shows that the combination of high shell coverage and σ value results in a very similar increase of the shear velocity threshold compared to the wind tunnel experiments presented by McKenna Neuman et al. (2012).

The reason that the model calibration resulted in this particular value for σ is that the model does not differentiate between the fluid and impact velocity threshold. Therefore, the roughness elements in the model affect the initiation of sediment transport equal to the continuation of sediment transport. The potential reduction in sediment availability increases with a decreasing value for σ (if $m = 0.5$, Figure 12) and is implemented through an increase in shear velocity threshold. The shear velocity threshold also affects aeolian sediment already in transport and originating from upwind, unarmored beach areas, like the mixed zones. Sediments from upwind areas are therefore partially deposited in the aeolian zone as soon a beach armor layer develops. For low values for σ the local deposition of sediment from upwind areas is already significant with low shell coverage. Low σ values therefore reduce the total sediment accumulation in the dunes quickly. In order for the model to provide reasonable total sediment transport rates, a higher value for σ was found in the calibration that ultimately induces a higher shell coverage. The value for σ therefore does not only represent a spatiotemporal averaged emergence of roughness elements, but also a compromise between its effect on the fluid and impact velocity threshold.

Note that the model conceptually allows to differentiate between the impact and fluid threshold. The right-hand side of the advection equation (Equation 2) can be modified according to:

$$E_k - D_k = \min \left(\frac{\partial m_{a,k}}{\partial t} \quad ; \quad \frac{\hat{w}_k}{T} \cdot [(1 - S_k) \cdot c_{\text{sat},k}^{\text{fluid}} + S_k \cdot c_{\text{sat},k}^{\text{impact}} - c_k] \right) \quad (10)$$

where $c_{\text{sat},k}^{\text{fluid}}$ [kg/m²] and $c_{\text{sat},k}^{\text{impact}}$ [kg/m²] are the sediment transport capacity associated with the fluid and impact threshold respectively and S_k [-] is the

degree of saturation.

Unfortunately, empirical data to quantify the differentiation is lacking. This potential model improvement is therefore still hypothetical and requires fundamental research on the impact and fluid shear velocity threshold under varying conditions.

7. Conclusions

The hindcast of the morphological development of the Sand Motor mega nourishment shows that the aeolian sediment transport and availability model AEOLIS captures the particular supratidal morphodynamic behaviour associated with mega nourishments. The supratidal morphodynamic behaviour at the Sand Motor is characterized by the significant compartmentalization, modest aeolian sediment transport rates and relatively low dune growth rates. The reduction of aeolian sediment availability due to soil moisture and beach armoring in the aeolian zone results in compartmentalization. Compartmentalization explains the major importance of the intertidal beach area as supplier of aeolian sediment and can largely explain the relatively low accumulation volumes in the Sand Motor domain when compared to adjacent coasts. The model also reflects the minor importance of the beach widths up to 1 kilometer that are present at the Sand Motor.

From the hindcast the following conclusions can be drawn:

- The AEOLIS model is able to reproduce multi-annual aeolian sediment transport rates in the Sand Motor domain in the four years after its construction with a RMSE of $3 \cdot 10^4 \text{ m}^3$ (7% of the total sediment accumulation of $40 \cdot 10^4 \text{ m}^3$) and R^2 of 0.93 when time series of measured and modeled total aeolian sediment transport volumes are compared.
- The AEOLIS model is able to reproduce large scale spatial patterns in aeolian sediment transport in the Sand Motor domain in the four years after its construction, but underestimates the deposition in the dune lake and lagoon, likely due to wind setup and groundwater seepage that are not yet included in the model.
- The AEOLIS model overestimates the total sedimentation volume with 5% on average, but underestimates the total sedimentation volume with 12% at the end of the simulation. The discrepancy at the end of the

simulation might be caused by a particularly dry season as precipitation is not enabled in the simulations.

- The AEOLIS model is able to capture the seasonal variations in sediment transport in all years, except for early 2014 when significant morphological change is possibly related to hydrodynamic sediment transport that is not included in the simulations.
- The AEOLIS model overestimates the shell coverage, which compensates the high value for σ . The high σ value is a compromise between the fluid and impact threshold that are currently assumed to be equal.

From the hindcast the following general conclusions can be drawn regarding spatiotemporal variations in aeolian sediment availability and transport and beach compartmentalization:

- The combination of spatial and temporal variations in aeolian sediment availability, due to the combined influence of soil moisture, sediment sorting and beach armoring, and the feedback between aeolian sediment availability and transport is essential for an accurate estimate of the total sedimentation volume at coastal sites where beach compartmentalization is present.
- Compartmentalization of the beach due to beach armoring should be taken into account when designing (mega) nourishments as it can govern aeolian sediment availability and transport.
- Compartmentalization of the beach can influence the lifetime and region of influence of a (mega) nourishments as it governs the wind-driven erodibility of the mega nourishment.

Acknowledgements

The work discussed in this paper is supported by the ERC-Advanced Grant 291206 – Nearshore Monitoring and Modeling (NEMO) and Deltares.

A. Model settings

The model schematizations presented in this paper used the settings listed below. Some model settings belong to experimental features of the model and are not discussed. These settings are listed for completeness only and marked with an asterisk (*). The model settings are chosen such that experimental features are disabled.

Parameter	Value
A	0.085
CFL	1.0
Cb	1.5
T	1.0
Tdry	5400.0
Tsalt*	0.0
accfac	1.0
bedupdate	False
beta	130.0
bi	0.05
boundary_lateral	circular
boundary_offshore	noflux
boundary_onshore	gradient
callback	None
cpair	0.0010035
csalt*	0.035
dt	3600.0
eps	0.001
evaporation	True
facDOD	0.1
g	9.81
gamma	0.5
grain_dist	0.005709 0.234708 0.608887 0.099666 0.001029 0.000001 0.010486 0.028503 0.010486 0.000522 0.000004
grain_size	0.000177 0.000250 0.000354 0.000500 0.000707 0.001000 0.002000 0.004000 0.008000 0.016000 0.032000
k	0.01
layer_thickness	0.01

Parameter	Value	(continued)
m	0.5	
max_error	0.000001	
max_iter	1000	
method_moist	belly_johnson	
method_transport	bagnold	
mixtoplayer	True	
nfractions	11	
nlayers	10	
output_times	604800.0	
porosity	0.4	
restart	None	
rhoa	1.25	
rhop	2650.0	
rhow	1025.0	
runup	False	
scheme	euler_backward	
sigma	11.9	
th_bedslope	False	
th_grainsize	True	
th_humidity*	False	
th_moisture	True	
th_roughness	True	
th_salt*	False	
tstart	0.0	
tstop	126230400.0	
z	10.0	

References

- Aagaard, T. (2014). Sediment supply to beaches: Cross-shore sand transport on the lower shoreface. *Journal of Geophysical Research*, 119(4):913–926. doi:10.1002/2013JF003041. 2013JF003041.
- Arens, S. M. (1996). Patterns of sand transport on vegetated foredunes. *Geomorphology*, 17:339–350.
- Baas, A. C. (2002). Chaos, fractals and self-organization in coastal ge-

- omorphology: simulating dune landscapes in vegetated environments. Geomorphology, 48(1-3):309–328. doi:10.1016/S0169-555X(02)00187-3.
- Bagnold, R. (1937). The transport of sand by wind. Geographical journal, pages 409–438.
- Bauer, B. O. and Davidson-Arnott, R. G. D. (2002). A general framework for modeling sediment supply to coastal dunes including wind angle, beach geometry, and fetch effects. Geomorphology, 49:89–108. doi:10.1016/S0169-555X(02)00165-4.
- Belly, P. Y. (1964). Sand movement by wind. Technical Report 1, U.S. Army Corps of Engineers CERC, Vicksburg, MS. 38 pp.
- Davidson-Arnott, R. G. D. and Bauer, B. O. (2009). Aeolian sediment transport on a beach: Thresholds, intermittency, and high frequency variability. Geomorphology, 105:117–126. doi:10.1016/j.geomorph.2008.02.018.
- Davidson-Arnott, R. G. D., Yang, Y., Ollerhead, J., Hesp, P. A., and Walker, I. J. (2008). The effects of surface moisture on aeolian sediment transport threshold and mass flux on a beach. Earth Surface Processes and Landforms, 33(1):55–74. doi:10.1002/esp.1527.
- de Schipper, M. A., de Vries, S., Ruessink, G., de Zeeuw, R. C., Rutten, J., van Gelder-Maas, C., and Stive, M. J. (2016). Initial spreading of a mega feeder nourishment: Observations of the sand engine pilot project. Coastal Engineering, 111:23–38. doi:10.1016/j.coastaleng.2015.10.011.
- de Vries, S., Arens, S. M., de Schipper, M. A., and Ranasinghe, R. (2014a). Aeolian sediment transport on a beach with a varying sediment supply. Aeolian Research, 15:235–244. doi:10.1016/j.aeolia.2014.08.001.
- de Vries, S., Radermacher, M., de Schipper, M., and Stive, M. (2015). Tidal dynamics in the Sand Motor lagoon. In E-proceedings of the 36th IAHR World Congress.
- de Vries, S., van Thiel de Vries, J. S. M., van Rijn, L. C., Arens, S. M., and Ranasinghe, R. (2014b). Aeolian sediment transport in supply limited situations. Aeolian Research, 12:75–85. doi:10.1016/j.aeolia.2013.11.005.

- Durán, O. and Moore, L. J. (2013). Vegetation controls on the maximum size of coastal dunes. Proceedings of the National Academy of Sciences of the United States of America, 110:17217–17222. doi:10.1073/pnas.1307580110.
- Dyer, K. R. (1986). Coastal and estuarine sediment dynamics. Wiley, Chichester.
- Hoonhout, B. M. and de Vries, S. (2016). A process-based model for aeolian sediment transport and spatiotemporal varying sediment availability. Journal of Geophysical Research: Earth Surface. doi:10.1002/2015JF003692. 2015JF003692.
- Hoonhout, B. M. and de Vries, S. (2017). Aeolian sediment supply at a mega nourishment. Coastal Engineering. doi:10.1016/j.coastaleng.2017.03.001. Submitted.
- Horikawa, K., Hotta, S., Kubota, S., and Katori, S. (1983). On the sand transport rate by wind on a beach. Coastal Engineering in Japan, 26:101–120.
- Hotta, S., Kubota, S., Katori, S., and Horikawa, K. (1984). Sand transport by wind on a wet sand beach. In Proceedings of the 19th Conference on Coastal Engineering, pages 1264–1281, Houston, TX. ASCE.
- Howard, A. D. (1977). Effect of slope on the threshold of motion and its application to orientation of wind ripples. Geological Society of America Bulletin, 88(6):853–856. doi:10.1130/0016-7606(1977)88;853:EOSOTT;2.0.CO;2.
- Huisman, B., De Schipper, M., and Ruessink, B. (2016). Sediment sorting at the sand motor at storm and annual time scales. Marine Geology, 381:209–226. doi:10.1016/j.margeo.2016.09.005.
- Jackson, D. W. T. and Cooper, J. A. G. (1999). Beach fetch distance and aeolian sediment transport. Sedimentology, 46:517–522. doi:10.1046/j.1365-3091.1999.00228.x.
- Jackson, N. L. and Nordstrom, K. F. (1998). Aeolian transport of sediment on a beach during and after rainfall, wildwood, nj, usa. Geomorphology, 22(2):151–157. doi:10.1016/S0169-555X(97)00065-2.

- Johnson, J. W. (1965). Sand movement on coastal dunes. Technical Report 570, Symp. 3, Paper no. 75, U.S. Department of Agriculture, Washington. pp 747-755.
- Kawamura, R. (1951). Study of sand movement by wind. Technical Report HEL-2-8, Hydraulics Engineering Laboratory, University of California, Berkeley.
- Keijsers, J., De Groot, A., and Riksen, M. (2016). Modeling the biogeomorphic evolution of coastal dunes in response to climate change. Journal of Geophysical Research: Earth Surface, 121(6):1161–1181. doi:10.1002/2015JF003815.
- King, J., Nickling, W. G., and Gillies, J. A. (2005). Representation of vegetation and other nonerodible elements in aeolian shear stress partitioning models for predicting transport threshold. Journal of Geophysical Research, 110(F4). doi:10.1029/2004JF000281. F04015.
- Kroy, K., Sauermann, G., and Herrmann, H. J. (2002). Minimal model for sand dunes. Physical Review Letters, 88(5):054301. doi:10.1103/PhysRevLett.88.054301.
- Lettau, K. and Lettau, H. (1978). Exploring the World's Driest Climate., chapter Experimental and micrometeorological field studies of dune migration., pages 110–147. University of Wisconsin - Madison. IES Report 101,.
- Lynch, K., Jackson, D. W. T., and Cooper, J. A. G. (2008). Aeolian fetch distance and secondary airflow effects: the influence of micro-scale variables on meso-scale foredune development. Earth Surface Processes and Landforms, 33(7):991–1005. doi:10.1002/esp.1582.
- McKenna Neuman, C., Li, B., and Nash, D. (2012). Microtopographic analysis of shell pavements formed by aeolian transport in a wind tunnel simulation. Journal of Geophysical Research, 117(F4). doi:10.1029/2012JF002381. F04003.
- Nickling, W. G. and Ecclestone, M. (1981). The effects of soluble salts on the threshold shear velocity of fine sand. Sedimentology, 28:505–510.

- Peckham, S. D., Hutton, E. W. H., and Norris, B. (2013). A component-based approach to integrated modeling in the geosciences: The design of CSDMS. Computers and Geosciences, 53:3–12. doi:10.1016/j.cageo.2012.04.002.
- Radermacher, M., de Schipper, M. A., Swinkels, C., MacMahan, J. H., and Reniers, A. J. (2017). Tidal flow separation at protruding beach nourishments. Journal of Geophysical Research: Oceans, 122(1):63–79. doi:10.1002/2016JC011942.
- Raupach, M., Gillette, D., and Leys, J. (1993). The effect of roughness elements on wind erosion threshold. Journal of Geophysical Research: Atmospheres, 98(D2):3023–3029. doi:10.1029/92JD01922.
- Sherman, D. J., Jackson, D. W., Namikas, S. L., and Wang, J. (1998). Wind-blown sand on beaches: an evaluation of models. Geomorphology, 22(2):113–133. doi:10.1016/S0169-555X(97)00062-7.
- Sherman, D. J. and Li, B. (2012). Predicting aeolian sand transport rates: a reevaluation of models. Aeolian Research, 3(4):371–378. doi:10.1016/j.aeolia.2011.06.002.
- Stive, M. J. F., de Schipper, M. A., Luijendijk, A. P., Aarninkhof, S. G. J., van Gelder-Maas, C., van Thiel de Vries, J. S. M., de Vries, S., Henriquez, M., Marx, S., and Ranasinghe, R. (2013). A new alternative to saving our beaches from sea-level rise: the Sand Engine. Journal of Coastal Research, 29(5):1001–1008. doi:10.2112/JCOASTRES-D-13-00070.1.
- Stockdon, H. F., Holman, R. A., Howd, P. A., and Sallenger, A. H. (2006). Empirical parameterization of setup, swash, and runup. Coastal engineering, 53(7):573–588. doi:10.1016/j.coastaleng.2005.12.005.
- Van Boxel, J., Arens, S., Van Dijk, P., et al. (1999). Aeolian processes across transverse dunes. i: Modelling the air flow. Earth Surface Processes and Landforms, 24(3):255–270. doi:10.1002/(SICI)1096-9837(199903)24:3<255::AID-ESP962>3.0.CO;2-3.
- Van Dijk, P., Arens, S., Van Boxel, J., et al. (1999). Aeolian processes across transverse dunes. ii: Modelling the sediment transport and profile development. Earth surface processes and landforms, 24(4):319–333. doi:10.1002/(SICI)1096-9837(199904)24:4<319::AID-ESP963>3.3.CO;2-D.

Weng, W. S., Hunt, J. C. R., Carruthers, D. J., Warren, A., and Wiggs, G. F. S. (1991). Air flow and sand transport over sand-dunes. Acta Mechanica, 2:1–22.